Accepted for publication in Bulletin of Volcanology, 27 May 2015

DOI 10.1007/s00445-015-0943-x

A five thousand year record of multiple highly explosive mafic eruptions from Gunung Agung (Bali, Indonesia): Implications for eruption frequency and volcanic hazards

Karen Fontijn[1,2,3,*], Fidel Costa[1], Igan Sutawidjaja[4], Christopher G. Newhall[1,5], Jason S. Herrin[1,6]

[1] Earth Observatory of Singapore, Nanyang Technological University, 50 Nanyang Avenue, N2-01, Singapore 639798, Singapore

[2] Department of Earth Sciences, University of Oxford, South Parks Road, Oxford OX1 3AN, UK

[3] Department of Geology and Soil Science, Ghent University, Krijgslaan 281 – S8, 9000 Ghent, Belgium

[4] Centre for Volcanology and Geological Hazard Mitigation, Geological Agency, Jalan Diponegoro 57, Bandung – 40122, Indonesia

[5] *Now at* Mirisbiris Garden and Nature Center, Salvacion, Sto Domingo, Albay, 4508 Philippines

[6] Facility for Analysis Characterisation Testing Simulation, School of Materials, Science & Engineering, Nanyang Technological University, Nanyang Drive, N4.1 B4-10, Singapore 639798, Singapore

*Corresponding author: Karen Fontijn, Karen.Fontijn@earth.ox.ac.uk, tel. +44 1865 272045

Abstract

The 1963AD eruption of Agung volcano was one of the most significant 20th century eruptions in Indonesia, both in terms of its explosivity (Volcanic Explosivity Index (VEI) of 4+) and its short-term climatic impact as a result of around 6.5 Mt SO_2 emitted during the eruption. Because Agung has a significant potential to generate more sulphur-rich explosive eruptions in the future, and in the wake of reported geophysical unrest between 2007 and 2011, we investigated the Late Holocene tephrostratigraphic record of this volcano using stratigraphic logging, and geochemical and geochronological analyses. We show that Agung has an average eruptive frequency of one VEI ≥2-3 eruption per century. The Late Holocene eruptive record is dominated by basaltic andesitic eruptions generating tephra fall and pyroclastic density currents. About 25% of eruptions are of similar or larger magnitude than the 1963AD event, and this includes the previous eruption of 1843AD (estimated VEI 5, contrary to previous estimations of VEI 2). The latter represents one of the chemically most evolved products (andesite) erupted at Agung. In the Late Holocene, periods of more intense explosive activity alternated with periods of background eruptive rates similar to those at other subduction zone volcanoes. All eruptive products at Agung show a texturally complex mineral assemblage, dominated by plagioclase, clinopyroxene, orthopyroxene and olivine, suggesting recurring open-system processes of magmatic differentiation. We propose that erupted magmas are the result of repeated intrusions of basaltic magmas into basaltic andesitic to andesitic reservoirs producing a hybrid of bulk basaltic andesitic composition with limited compositional variations.

Keywords

Agung, tephrostratigraphy, eruptive history, basaltic andesite, magma mixing, magma mingling

Introduction

A detailed view of the eruptive history of a volcano provides crucial information for hazard assessment at different timescales. Historical records of volcanic activity typically only span a few hundred years, depending on the geographic location. In the case of frequently erupting volcanoes, these historical records are sufficient for a relatively good understanding of the typical style of activity at a specific volcano in its current state, and thus short-to-mid-term hazards, e.g. the case for 20th century dome-forming eruptions at Merapi (Voight et al. 2000). Even at frequently active volcanoes however, historical records may be far from complete, as was recently demonstrated for Villarrica volcano in Chile, based on a high-resolution temporal record of tephra and lahar deposits entrained in lacustrine sediments (Van Daele et al. 2014). Mid-to-long-term hazard assessment especially requires information from geological, typically tephrostratigraphic, studies which may highlight (long-term) temporal variations in magma composition, eruptive style and/or frequency, and associated hazards (e.g. for Merapi: Andreastuti et al. 2000; Gertisser et al. 2012; Newhall et al. 2000). At dormant volcanoes with only few or no historically documented eruptions, tephrostratigraphy is the primary source of information for volcanic hazard assessment, which feeds into risk management and mitigation plans. In this paper, we present the first tephrostratigraphic record for Gunung (Indonesian for hill or mountain) Agung volcano in eastern Bali, to understand the past and potential future behaviour of this highly explosive basaltic andesite volcano.

Gunung Agung is part of the Sunda volcanic arc, and forms the highest peak (3142 m a.s.l.) on Bali, surrounded by the major calderas of Bratan (Ryu et al. 2013) and Batur (Reubi and Nicholls 2004a; Sutawidjaja 2009) to the west (Fig 1), and the Rinjani – Samalas complex (Lavigne et al. 2013) on Lombok to the east. Agung is of sacred importance to the Balinese people, who hold ceremonies and make offerings to the volcano on a regular basis.

Historical texts describing Balinese history mention eruptions in the 16th–18th centuries, with a notably calamitous event in 1711AD that caused several hundreds of deaths and destruction on all sides of the volcano (Hägerdal 2006). Agung also had explosive eruptions in 1808AD, 1821AD (uncertain, possibly mistaken for an eruption from neighbouring Batur) and 1843AD, for which little or no detail is known from historical accounts. All two/three 19th century eruptions are considered VEI (Volcanic Explosivity Index; Newhall and Self 1982) 2 events (Siebert et al. 2010), although we provide evidence here that the 1843AD eruption must have been significantly larger (VEI 5, i.e. three orders of magnitude larger than previously thought). The 1843AD eruption was reported to be preceded by felt earthquakes and to have dispersed "sand, ash and stones" (Zollinger 1843, reported in Piip et al. 1963; Zen and Hadikusumo 1964).

In 1963 Agung had one of the biggest 20th century eruptions worldwide (Self and Rampino 2012). After a few days of felt earthquakes and small ash eruptions in February 1963, ~0.1 km^3 of andesite lava was extruded until 17th March, when a large explosive eruption generated pyroclastic density currents (PDCs) and lahars, and devastated a wide area predominantly north and south of the volcano. A second explosive phase of similar intensity occurred two months later, on 18th May, producing more PDCs and lahars. The total death toll of the eruption is estimated between 1100 and 1900 (Self and Rampino 2012; Tanguy et al. 1998; Zen and Hadikusumo 1964). Intermittent, smaller, explosions continued until 20th June 1963 (Piip et al. 1963), and secondary lahars were generated for several months after the end of the eruption. A total estimated magma volume of ca. 0.4 km^3 was erupted (Self and Rampino 2012), corresponding to a magnitude 5.0 eruption (Pyle 2000); the bulk volume of pyroclastics (ca. 0.8 km^3; Self and Rampino 2012) make this a high-end VEI 4 event (Newhall and Self 1982). Self and King (1996) inferred from petrological and geochemical data that a basaltic intrusion mixed into an andesitic reservoir. The 1963AD eruption was one

of the first witnessed volcanic eruptions that had a short-lived climatic impact due to vast amounts of sulphur being injected into the higher atmosphere, where it formed 10–12 Mt of H_2SO_4 aerosols (Self and Rampino 2012). Estimated global average temperature decreases as a result of these aerosols in the months to years after the eruption, vary from 0.1 to 0.4 °C (Angell and Korshover 1985; Canty et al. 2013; Rampino and Self 1982; Self et al. 1981; Wigley et al. 2005).

In 1989 weak solfataric activity and a few volcanic earthquakes were reported (Global Volcanism Program, http://volcano.si.edu). Apart from those, Agung has been largely quiet since 1963. Based on ALOS Interferometric Synthetic Aperture Radar data, Chaussard et al. (2013) reported inflation centred on the volcano's summit at a rate of 7.8 cm/yr between mid-2007 and early 2009, followed by slow deflation (and no eruption) at a rate of 1.9 cm/yr until mid-2011 (the last acquired data). The 2007–2009 inflation was modelled to result from a shallow source ca. 4.4 km below Agung's summit, or 1.9 km below the average base level of the volcano, and could reflect the addition of new magma in the shallow storage levels (Chaussard and Amelung 2012). The deflation may be explained by cooling and thermal contraction of the magma (Chaussard et al. 2013), or by passive degassing of magma that was injected up until 2009 (Girona et al. 2014). Based on the evidence of active deformation, in 2012 and 2013 a GPS and new seismic network was installed at Agung by the Indonesian Centre for Volcanology and Geological Hazard Mitigation and the United States Geological Survey Volcano Disaster Assistance Program. To date, little significant deformation or seismicity has been detected (J Pallister, personal communication 2015).

Previous studies of Agung have focused mostly on the 1963AD event (Self and King 1996; Self and Rampino 2012) and its climatic impact (e.g. Rampino and Self 1982). From the geological map by Nasution et al. (2004) it is clear that Agung has a history of repeated eruptions generating lava flows, PDCs and lahars. Unlike at its immediate neighbours, there

is no geological evidence to suggest that Agung had a caldera-forming event in its past. This study evaluates the Holocene eruptive frequency – magnitude relationships at Agung using the stratigraphy of pyroclastic deposits, and aims to put constraints on the magma plumbing system from petrological and geochemical data on products from some major eruptions.

Methodology

Stratigraphic logging and sampling of pyroclastic fall and PDC deposits was carried out on all sides of Agung in 52 locations. Sequences of pyroclastic fall deposits were mostly found on the western side of the volcano, in the saddle between Agung and Batur (Fig 1). Stacks of PDC deposits were mainly studied in quarries on the southern and northern flanks of Agung. Samples of well-preserved deposits were taken for petrological and geochemical analysis. Charcoal enclosed in PDC deposits and palaeosols between fall deposits was sampled for radiocarbon dating, performed at Beta Analytic Inc. (Florida, USA). Thirty samples were dated, either by the conventional radiometric method or by accelerator mass spectrometry, depending on the amount of material available (Table 1).

Polished thin sections of individual scoria and pumice lapilli from fall deposits, scoriaceous bombs from PDC deposits, and a few pieces of lava, were prepared at High Mesa Petrographics (New Mexico, USA). Bulk geochemical analysis was performed at Activation Laboratories Ltd. (Ontario, Canada). When possible, individual scoria or pumice lapilli were selected for these bulk analyses. In other cases multiple lapilli were grouped to obtain enough material for a representative bulk analysis. Samples were first powdered in a mild steel mill, after which Loss on Ignition was determined. Major elements and selected trace elements were analysed with Inductively Coupled Plasma – Optical Emission Spectroscopy (ICP-OES) using lithium-metaborate flux melting to dissolve the powders. Other trace elements were

analysed with ICP – Mass Spectroscopy (ICP-MS). Bulk geochemical data are presented in Supplementary Table 1.

Major and minor element composition of phenocrysts was obtained on thin sections and grain mounts of selected samples with a JEOL JXA 8530-F Field Emission Electron Microprobe (EMP) equipped with 5 tuneable wavelength-dispersive spectrometers at the Facility for Analysis, Characterisation, Testing and Simulation at Nanyang Technological University, Singapore. Point analyses on pyroxene, olivine and magnetite were acquired using a focused beam, 20nA beam current and 15kV accelerating voltage. Beam current was reduced to 10nA for plagioclase and glass (melt inclusions), which were analysed with a beam diameter of 3 and 5 μm respectively. Cl and S were measured at a 50nA current in glass at the end of each analysis. Peak and off-peak counting times varied between 20s and 40s, depending on expected concentration. Results were quantified using well-characterised natural and synthetic external calibration standards and a modified ZAF matrix correction procedure. A time-dependent intensity correction was applied to analyses of plagioclase and glass to correct for beam modification of the sample during analysis. Amphibole was not present in sufficient quantities for reliable analysis. The groundmass of many samples was too crystal-rich to allow for matrix glass analysis. EMP data are presented in Supplementary Table 2a-e.

Stratigraphy and bulk geochemistry of pyroclastic deposits

Individual tephra fall and PDC units were correlated wherever possible using a combination of stratigraphic, petrological, geochemical and geochronological constraints. We assumed at first, and later proved geochemically, that scoria fall deposits in sections west of Agung result from Agung due to dominantly easterly winds dispersing tephra to the west. Almost no tephra fall deposits are preserved on the eastern flank of the volcano. PDC deposits found in quarries

on all sides of the volcano are also interpreted to originate from Agung, based on their spatial distribution and their geochemical composition which is distinct from Batur deposits. Schematic logs of representative sections exposing tephra fall and PDC deposits (Fig 2), with suggested correlations, are shown in Figure 3.

The oldest radiocarbon date we obtained on a palaeosol in the tephra fall sequences is 5.16±0.09 cal. ka BP (Sample AG024B; Table 1, Fig 3). The combined tephra fall sections provide a record of Late Holocene explosive eruptions that were large enough to be preserved. The oldest radiocarbon date on charcoal from a PDC deposit is 5.95±0.05 cal. ka BP (Table 1, Fig 3). The latter is however separated by a stratigraphic discordance (stream deposits) from the deposits higher up in the sequence. Most PDC deposits studied here were emplaced within the last 1200 years.

Agung's Late Holocene stratigraphy is dominated by scoria fall deposits of medium-K basaltic to basaltic andesitic composition (Fig 4; classification following Peccerillo and Taylor (1976)). Occasional andesitic pumice fall deposits or dispersed fine pumice lapilli in palaeosols also occur. These pumice fall deposits are usually poorly preserved and we could only obtain geochemical data for the three most recent ones, including the one we interpret to be associated with the 1843AD eruption (see further). There is no evidence for large Plinian-style fall or ignimbrite deposits at Agung, in contrast to Batur (Reubi and Nicholls 2004a; Sutawidjaja 2009).

PDC deposits are generally more evolved than scoria fall deposits, spanning a compositional range from basaltic andesite to andesite, similar to that displayed by the 1963AD eruptive products, from the lava flow to the most mafic scoria fall deposits (Fig 4; Self and King 1996). This compositional spread between types of deposits, the lack of a glassy groundmass, and the compositional range displayed by one eruption (1963AD) makes it difficult to firmly correlate units. In addition, the tephra fall sequences tend to sample a

different timeframe than the PDC sequences. The only Agung deposits we confidently correlate between multiple locations, apart from the 1963AD deposits which occur in the topsoil, are the underlying pumice fall and PDC units of the 1843AD eruption. This correlation is based on the characteristic andesitic chemical composition (Supplementary Table 1) as well as radiocarbon ages that are consistent with the historical age of the eruption (Table 1). The 120±40 ^{14}C yr BP Aap5 PDC unit defined by Nasution et al. (2004; ^{14}C date after Doust 2003), occurring to the NE of Agung, most likely also corresponds to the same event. Nasution et al. (2004) also defined a pyroclastic fall unit with scoria, pumice and lithic lapilli (Ajp1), which stratigraphically underlies the 1963AD PDC deposits (Aap6). Based on its stratigraphic position and description, this Ajp1 unit likely corresponds to the 1843AD fall deposit, although its thickness distribution is poorly constrained. The chemical composition of the second-most recent lava flow, Al13 (Nasution et al. 2004) also matches well with that of our 1843AD deposits (Doust 2003). Our new localities where the 1843AD deposits are found significantly expand their previously known spatial distribution (Fig 5). PDC deposits occur on all sides of the volcano, and suggest a similarly widespread distribution than that of the 1963AD PDC deposits. The 1843AD fall deposit thickness of 40 to 70 cm also suggests an eruption size at least comparable to, and probably larger than, the 1963AD one (Self and Rampino 2012).

The chemical composition of the 1843AD products is similar to that of the 1963AD lava flow (Fig 4 and 6), which was the first to erupt before scoria falls and PDCs (Self and King 1996). This could suggest that the 1963AD andesitic lava flow was a leftover of the 1843AD magma, and would be consistent with the triggering mechanism for the 1963AD eruption proposed by Self and King (1996), i.e. mixing of basaltic magma into an existing andesitic reservoir.

Andesitic to (trachy)dacitic pumice fall and PDC deposits interbedded within the scoria fall sequence (Fig 3) are interpreted to originate from Batur Plinian-style eruptions, as confirmed by their chemical composition (Fig 4, 6, Supplementary Table 1; Reubi and Nicholls 2005). Although the major element compositions of some Batur samples are similar to those of some Agung samples, especially in the basaltic andesite range (Fig 4), certain trace element ratios, e.g. Zr/Nb, are useful to distinguish deposits from Agung and Batur (Fig 6). We attribute these subtle differences in trace element signature between Agung and Batur to differences in the source rock components and/or the degree of partial melting generating the parent melts beneath both volcanoes (e.g. Reubi and Nicholls 2004b). The trace element signatures confirm that all scoria fall deposits and the few andesitic units we identified in the studied sequences, all downwind of Agung and upwind of Batur, originate from Agung. The latter include pumice at the surface and a PDC unit S of Agung (samples AG001bisH, AG045D; Supplementary Table 1, Fig 3), which chemically corresponds well with the Aap3 unit defined on the geological map (Doust 2003; Nasution et al. 2004) This andesitic PDC deposit represents the most evolved composition found for Agung and is chemically clearly distinct from the 1843AD products. It was dated at 0.17±0.10 ka cal BP (sample AG045E; Table 1) and could correspond to the 1808AD eruption.

A twin fine-grained cream-coloured pumice fall unit which clearly stands out from Agung deposits has proven a useful marker horizon in several key sections. We interpret this unit as the 1257AD pumice fall deposit from the neighbouring Rinjani – Samalas complex on Lombok. This is consistent with both its geochemical composition and radiocarbon ages bracketing the deposit age (Fig 3, Table 1, Supplementary Table 1; Lavigne et al. 2013).

Petrography and mineralogy

All studied samples from Agung are petrologically complex, with signs of open-system processes (Fig 7 and 8). Scoria fall samples generally show a porphyritic texture, with only few microphenocrysts in a moderately vesicular brown to black groundmass (Fig 7a). Scoriaceous bombs and blocks from PDC deposits have a seriate texture with a crystallised, poorly to moderately vesicular groundmass and little glass (Fig 7b-d). The most evolved samples (>55% SiO_2) contain, in varying proportions, porphyritic inclusions with a lighter-coloured and more vesicular groundmass than the bulk of the material, but with similar mineralogical assemblage (Fig 7c). The mineralogical assemblage is dominated by plagioclase, followed by clinopyroxene, orthopyroxene and titanomagnetite. Most samples also contain olivine and accessory apatite (sometimes included in pyroxene or titanomagnetite). Rare amphibole is found in the most evolved samples, and tends to have breakdown rims a few tens of micrometres wide.

To quantify mineral compositions using EMP analyses, we selected samples from the three most recent PDC deposits from section AG042-042bis (Fig 3), spanning the compositional range for PDCs found at Agung, ca. 53–56% SiO_2, including the 1843AD deposits. For the scoria fall samples, we focus on the major deposits from section AG008-021 as it is the most complete section for the Late Holocene and we can correlate it well to section AG042-042bis (Fig 3). Again, this selection of samples spans almost the entire compositional range of fall deposits found at Agung: ca. 51.5–57.5% SiO_2.

Plagioclase

Plagioclase shows a variety of zoning patterns, including normal, reverse and oscillatory zoning (Fig 8a-b). The larger crystals, up to 1–1.5 mm in size, often have a sieve-textured core and a clear oscillatory zoned rim, especially in the basaltic to basaltic andesitic samples.

Sieve-textured plagioclase is less abundant in andesitic samples and in the light-coloured vesicular inclusions. Some plagioclase crystals show dissolution zones between a clear core and rim (Fig 8b). Clear, unzoned, sub- to euhedral plagioclase needles occur in the groundmass of all samples. Compositions range from An_{41} to An_{93} (Fig 9). Core compositions span this entire range in the most evolved samples (≥55wt% SiO_2), but tend to display a more narrow range in more mafic samples, from around An_{50-60} to An_{90}. In these latter samples, plagioclase cores tend to be more calcic than rims (Fig 9a-b). Plagioclase rims in nearly all samples display a more narrow range than cores, of ~An_{50-80} (Fig 9), a wider range than that reported for the 1963AD products by Self and King (1996).

Pyroxene

Clinopyroxene and orthopyroxene occur in roughly equal proportions but are less abundant than plagioclase. Some samples contain glomerocrysts with pyroxenes, olivine and titanomagnetite. Most clinopyroxenes have large cores, often with a patchy appearance, and narrow oscillatory zoned rims (Fig 8c-d). Apatite, titanomagnetite and melt inclusions are common. Most clinopyroxenes are sub- to euhedral, but in the most mafic samples they have some rounded edges or show signs of rim dissolution. Compositions range from $En_{39-49}Wo_{34-45}$ and thus classify as augite (Morimoto et al. 1988). Mg# [= 100 x Mg/(Mg + Fe*); Fe* is total iron] varies between 68 and 86 (Fig 10a-b), without a clear correlation with bulk SiO_2 content. There is very little variation between core and rim compositions (Fig 10a-b). Al_2O_3 contents generally vary between ca. 1.0 and 3.5wt%, with a few exceptions up to 5.9wt% in the more evolved samples.

In the most evolved samples, orthopyroxene mostly occurs with large cores, often with a patchy appearance, surrounded by relatively broad oscillatory zoned rims (Fig 8c). Apatite,

titanomagnetite and melt inclusions sometimes occur in the patchy cores. The contact between core and rim is usually sharp but can be irregular. In more mafic samples, crystal rims tend to be narrower or even absent, and sometimes show signs of dissolution or rounding. Compositions generally vary between $En_{65-74}Wo_{3-4}$, with Mg# = 67–79 (Fig 10c-d), except for the cores in the more evolved samples (especially the PDC ones), which tend to be less Mg-rich (as low as Mg# = 61, Fig 10d), and show a range in composition ($En_{59-71}Wo_{3-4}$). 1963AD orthopyroxene was also commonly found to be reversely zoned by Self and King (1996). In the other samples core and rim compositions show little or no variation.

Olivine

Olivine is found in most samples, except in some of the most evolved ones. It occurs as sub- to anhedral crystals, sometimes embayed, and often with reaction rims of orthopyroxene ($En_{68-71}Wo_{4-5}$, Mg# = 74–78; Fig 8e-f). Reaction rims are thin in the most mafic sample (AG042D). Sample AG042I, compositionally between AG042D and AG042B, contains embayed olivine with thick reaction rims of orthopyroxene, as well as subhedral olivine without reaction rims. Compositions generally vary from Fo_{71} to Fo_{80}. Scattered olivines in scoria fall samples show compositions mostly of Fo_{71-74}, with some exceptions (Fo_{57}, Fo_{62}) in one of the most mafic scoria fall samples. Cores are generally slightly more Mg-rich than rims (excluding reaction rims).

Melt inclusions

A few melt inclusions were found in pyroxene and olivine of the tephra fall samples. The inclusions do not contain vapour bubbles or secondary crystals. The glass composition is

generally basaltic andesitic to andesitic, and more evolved than the bulk composition of the host magma (Fig 4). Sulphur contents vary from 120 to 740 ppm, with a tendency for the higher values to occur in the more mafic melt inclusions. Chlorine contents range from 1900 to 3300 ppm, with higher values in the more evolved melt inclusions. These values are similar to those reported by Self and King (1996) in the 1963AD products.

Intensive variables

Pre-eruptive temperatures of touching pairs or intergrowths of clino- and orthopyroxene were estimated using QUILF (Andersen et al. 1993). In absence of other constraints on pressure, we set the input pressure at 123 MPa, corresponding to 4.4 km depth below the summit (using a crustal density 2800 kg/m^3), i.e. the depth of the modelled source of inflation from 2007 to 2009 by Chaussard and Amelung (2012). Pyroxene pairs were tested for equilibrium following Putirka (2008). Estimated temperatures for touching pairs in equilibrium vary between 976 and 1085°C, with a general tendency for temperatures to be lower in the more evolved samples. Even the most mafic sample shows relatively low temperatures as well, but we ascribe this to the limited number of touching pairs that were found in each sample (between 3 and 10 pairs per sample).

Discussion

Magmatic differentiation

Based on our dataset representing compositions erupted at Agung during the Late Holocene, we construct a generalised conceptual model of recurring magmatic processes at Agung

leading to highly frequent basaltic andesitic explosive activity. All samples show petrographical evidence of systematic magma mingling/mixing, generating the range of erupted magmas. This is particularly evidenced by the complex zoning patterns and wide range of compositions of plagioclase, suggestive of crystallisation, and occasional dissolution, under variable conditions of host melt composition, temperature, water content and/or pressure. Plagioclase crystals tend to look more pristine in andesitic samples than in more mafic samples, and rim compositions in all samples display a more narrow range than cores. Pyroxene compositions are less variable, but their textures are suggestive of a mafic component showing disequilibrium features, and a more evolved component with large cores and rims of a different composition. Olivine is unstable and recrystallizing to orthopyroxene in basaltic andesitic samples, but only shows a limited amount of dissolution in more mafic samples. All these textural observations together suggest that mingling of a basaltic (andesitic) magma and an andesitic magma to form a hybrid basaltic andesite is a ubiquitous process at Agung. During mingling both end-member magmas partially re-equilibrate with the new liquid composition and varying proportions of mingling components may lead to variations in the bulk composition of the hybrid magma over a limited compositional range.

The few analysed melt inclusions in olivine and pyroxene from Late Holocene fall deposits, suggest similar pre-eruptive levels of S and Cl in the melt to those reported for the 1963AD eruption, which produced an estimated 6.5 Mt of SO_2 (Self and King 1996; Self and Rampino 2012). If 25% of eruptions at Agung produce an amount of H_2SO_4 aerosols of the same order of magnitude (Section ”Eruption frequency and rate”), Agung is a significant source of regular, strong atmospheric perturbations.

Eruption style – hazards

The valleys S and SE of Agung are subjected to PDCs every ca. 250-300 years (Fig 1, 3). These are minimum estimates influenced by erosion, slope morphology and eruption particularities. The geological map suggests that the N-NE and SW-SE flanks are most prone to PDCs. Lava flows occur on all flanks of the volcano. The most silicic ones are generally restricted to the upper flanks, whereas the most mafic ones have reached the NE coastline (Nasution et al. 2004).

Most tephra fall deposits are more mafic than the PDC deposits, and it is not clear how the two types of deposits are linked in Agung's history. The fact that different sequences sample different time intervals complicates interpretations. In 1963AD, the PDCs were more mafic than the lava flow and early fall deposits (Self and King 1996), and in the case of the 1843AD eruption, all deposits have a similar geochemical composition. Those two eruptions were both associated with a lava flow, tephra fall as well as PDCs, but for older deposits, we cannot constrain whether all PDC deposits have associated fall deposits, and vice versa, or whether eruptions typically start with the effusion of a lava flow, as in 1963AD.

The majority of PDC deposits at Agung resulted from scoria flows, containing scoriaceous breadcrust bombs (e.g. AG042B). Some PDC deposits were identified as block-and-ash flow deposits (e.g. AG042D), which would typically result from gravitational collapse of a growing lava dome, as frequently happens at Merapi in central Java (e.g. Voight et al. 2000). The main juvenile component of these PDC deposits consists of dense decimetre-scale blocks of basaltic andesitic lava, set in a loose gritty ash matrix. Although the crystallinity of blocks originating from a lava dome could be expected to be higher than that of scoriaceous bombs due to slower cooling rates in the former (e.g. Sparks et al. 2000), a qualitative comparison of both types does not reveal significant differences in texture. All blocks and bombs from Agung PDC deposits however display similar crystallinities to blocks from Merapi PDC

deposits, which are clearly derived from lava dome collapse (Preece et al. 2013). Despite similarities in overall crystallinity, we did not spot any Ti-magnetite grains with exsolution lamellae that would result from stagnation in a shallow conduit (Turner et al. 2008), as seen for Merapi's 2010 samples (Preece et al. 2013), in any of the thin sections that were studied with backscatter secondary electron imaging. We cannot rule out that a lava dome could occasionally grow at Agung's summit, but based on the current dataset it does not seem likely that lava dome formation is a common process in Agung's geologically recent history.

Eruption frequency and rate

Fifty-two tephra-fall-producing eruptions are recognised in the last ca. 5.2 ky in combined sections AG008/021 and AG006/006bis (Fig 3). This represents an average eruptive frequency of 1 eruption every 100 years, seemingly consistent with the general frequency of eruptions described in historical texts covering the last ca. 500 years (Hägerdal 2006). We assigned an approximate age to each event, assuming the average eruptive frequency of one event per century has not changed significantly over time. This assumption seems valid from a qualitative inspection of the tephra fall sections (Fig 3).

With both reference sections AG008/021 and AG006/006bis 8-10 km downwind of Agung and only 3.5 km apart, we use deposit thickness and maximum grain size as a proxy of eruption size relative to that of the 1963AD eruption (thickness ~45cm, maximum grain size ~40mm), and assign an approximate VEI and associated volume to each event. This simplified approach assumes that the sections west of Agung capture the most complete history of tephra-fall-producing eruptions for Agung due to prevailing easterly winds. Sections east of Agung clearly contain much less, and much more poorly preserved, tephra

fall deposits, and sections north and south mostly comprise PDC deposits unlikely to provide a complete picture of eruptive histories due to potential erosion in underlying units during emplacement. Deposits which are clearly thicker and/or coarser than 1963AD at the type locality, e.g. 1843AD, are assigned VEI 5 and 1 km^3 (the lower VEI 5 limit; Newhall and Self 1982). Deposits of similar scale to 1963AD are assigned VEI 4 with 0.5 km^3, except for 1963AD itself, which is estimated to comprise 0.8 km^3 of tephra (Self and Rampino 2012). Events smaller than 1963AD are further subdivided into VEI 3 (0.05 km^3) and VEI 2 (0.005 km^3) using an arbitrary deposit thickness threshold of 10 cm.

In the Late Holocene, almost 10% of eruptions are significantly larger than the 1963AD one and more than 15% are of similar intensity. From our conservative volume and age estimates for each event, we obtain a normalised cumulative volume vs. time evolution for fall-producing eruptions (Fig 11), suggesting that Agung experienced a ~10-fold increase in magma eruptive rates between ~3.2 and 2.0 ka. Rates before and after this time interval averaged ~0.2–0.3 km^3/ky. During the ~3.2–2.0 ka interval they averaged ~ 2 km^3/ky. The most recent period of activity at Agung seems to be characterised by similarly high eruptive rates. The composition of the magmas leading to these volumetrically more important eruptions is not more evolved than in the calmer periods of activity, the only clear exception being the 1843AD eruption.

Reported eruptive rates for explosive activity over the last 0.1-10 kyrs at basaltic–andesitic subduction zone volcanoes range from 0.1–0.7 km^3/ky (e.g. Colima: Luhr and Carmichael 1982; Kuju: Kamata and Kobayashi 1997; Lamongan: Carn 2000; Aso: Miyabuchi 2009). Apparently, Agung has experienced periods of relatively high magma eruptive rates in its recent past, alternating with rates comparable to those seen at other similar volcanoes. The processes controlling the variable eruptive rates remain unclear. A regional tectonic influence resulting in partial blockage of the conduit or deeper plumbing systems seems

counterintuitive: we would expect to see (i) more evolved compositions in the higher-activity periods as a result of prolonged magmatic differentiation during calmer periods (e.g. seen at Merapi, Gertisser and Keller 2003b), and (ii) a similar response of reduced/increased activity to regional tectonic stress changes in neighbouring volcanoes. In contrast, it seems more likely that the Late Holocene history of Agung is characterised by periodic increased magma supply rates from depth, followed by limited crustal residence times, and resulting in frequent intense explosive activity of relatively mafic magmas.

Conclusions

The tephrostratigraphic record of Agung volcano shows that its eruptive activity in the Late Holocene was dominated by explosive eruptions generating moderately widespread tephra fall deposits, mainly impacting the east of Bali. Juvenile scoria of basaltic andesitic composition, as well as PDC deposits, are typically confined to the northern and southern slopes. These PDCs were commonly reworked to produce lahar nearer the coastline. The compositional range of eruptive products at Agung is limited to basaltic andesite, and occasionally andesite, e.g. the 1963AD lava flow and the 1843AD eruption. The latter is of at least similar magnitude to the 1963AD events, as are about 25% of the documented deposits. The complex petrographic relationships record evidence for systematic open-system magmatic differentiation. The most abundant mineral phases show textural and compositional evidence of a repeated history of basaltic intrusions into a slightly more evolved reservoir, possibly andesitic, producing hybrid basaltic andesitic magmas. S-rich melt inclusions suggest that Agung is a potential source of regular, and significant atmospheric perturbation by frequent emission of large amounts of SO_2. The tephra fall record suggests an average frequency of one explosive eruption per century, with some of the deep valleys along the southern flank of Agung subjected to PDCs every few centuries. At the millennium scale,

Agung is characterised by periods of background eruptive rates similar to other subduction zone volcanoes, alternated with periods of increased eruptive rates, ascribed to increased magma supply rates from depth.

Acknowledgements

We thank CVGHM for logistic support during fieldwork and RISTEK for research permits. We are grateful to Anwar Sidik, I Nengah Wardhana and Dewa Mertheyash from the Rendang Volcano Observatory for their hospitality and help in the field. Ryuta Furukawa is thanked for introductions to key outcrops. Tanya Furman is kindly acknowledged for sharing the work by Doust (2003). Reviews by John Pallister and Mary-Ann del Marmol, and editorial handling by James Gardner were greatly appreciated. Fieldwork and laboratory analyses were funded by the Earth Observatory of Singapore. Data interpretation and writing was performed at Oxford (NERC grant NE/I013210/1) and Ghent universities.

References

Andersen DJ, Lindsley DH, Davidson PM (1993) QUILF: A Pascal program to assess equilibria among Fe–Mg–Mn–Ti oxides, pyroxenes, olivine, and quartz. Computers & Geosciences 19:1333-1350

Andreastuti SD, Alloway BV, Smith IEM (2000) A detailed tephrostratigraphic framework at Merapi Volcano, Central Java, Indonesia: implications for eruption predictions and hazard assessment. J Volcanol Geotherm Res 100:51-67

Angell JK, Korshover J (1985) Surface Temperature Changes Following the Six Major Volcanic Episodes between 1780 and 1980. J Clim Appl Meteor 24:937-951

Bronk Ramsey C (2009) Bayesian analysis of radiocarbon dates. Radiocarbon 51:337-360

Canty T, Mascioli NR, Smarte MD, Salawitch RJ (2013) An empirical model of global climate – Part 1: A critical evaluation of volcanic cooling. Atmos Chem Phys 13:3997-4031

Carn SA (2000) The Lamongan volcanic field, East Java, Indonesia: physical volcanology, historic activity and hazards. J Volcanol Geotherm Res 95:81-108

Carr (2012) Igpet for Windows. http://home.comcast.net/~carrvolcano/site/?/page/Igpet_ for_Windows_and_M

Chaussard E, Amelung F (2012) Precursory inflation of shallow magma reservoirs at west Sunda volcanoes detected by InSAR. Geophys Res Lett 39:L21311

Chaussard E, Amelung F, Aoki Y (2013) Characterization of open and closed volcanic systems in Indonesia and Mexico using InSAR time series. J Geophys Res: Solid Earth 118:3957-3969

Costa F, Andreastuti S, Bouvet de Maisonneuve C, Pallister JS (2013) Petrological insights into the storage conditions, and magmatic processes that yielded the centennial 2010 Merapi explosive eruption. J Volcanol Geotherm Res 261:209-235

Doust R (2003) Volcanic hazard assessment Gunung Agung, Bali, Indonesia. Unpublished MSc Thesis, Pennsylvania State University.

Foden JD (1983) The Petrology of The Calcalkaline Lavas of Rindjani Volcano, East Sunda Arc: a Model for Island Arc Petrogenesis. J Petrol 24:98-130

Gertisser R, Charbonnier S, Keller J, Quidelleur X (2012) The geological evolution of Merapi volcano, Central Java, Indonesia. Bull Volcanol 74:1213-1233

Gertisser R, Keller J (2003a) Trace Element and Sr, Nd, Pb and O Isotope Variations in Medium-K and High-K Volcanic Rocks from Merapi Volcano, Central Java, Indonesia: Evidence for the Involvement of Subducted Sediments in Sunda Arc Magma Genesis. J Petrol 44:457-489

Gertisser R, Keller J (2003b) Temporal variations in magma composition at Merapi Volcano (Central Java, Indonesia): magmatic cycles during the past 2000 years of explosive activity. J Volcanol Geotherm Res 123:1-23

Girona T, Costa F, Newhall C, Taisne B (2014) On depressurization of volcanic magma reservoirs by passive degassing. J Geophys Res – Solid Earth 119:8667-8687.

Hägerdal H (2006) Candrasangkala: The Balinese art of dating events. University of Växjö, Sweden, 212 pp.

Jarvis A, Reuter HI, Nelson A, Guevara E (2008) Hole-filled seamless SRTM data V4, International Centre for Tropical Agriculture (CIAT), available from http://srtm.csi.cgiar.org.

Kamata H, Kobayashi T (1997) The eruptive rate and history of Kuju volcano in Japan during the past 15,000 years. J Volcanol Geotherm Res 76:163-171

Lavigne F, Degeai J-P, Komorowski J-C, Guillet S, Robert V, Lahitte P, Oppenheimer C, Stoffel M, Vidal CM, Surono, Pratomo I, Wassmer P, Hajdas I, Hadmoko DS, de Belizal E (2013) Source of the great A.D. 1257 mystery eruption unveiled, Samalas volcano, Rinjani Volcanic Complex, Indonesia. Proc Natl Acad Sci 110:16742-16747

Luhr JF, Carmichael ISE (1982) The Colima volcanic complex, Mexico:III. Contrib Mineral Petrol 80:262-275

Miyabuchi Y (2009) A 90,000-year tephrostratigraphic framework of Aso Volcano, Japan. Sedim Geol 220:169-189

Morimoto N, Fabries J, Ferguson AK, Ginzburg IV, Ross M, Seifert FA, Zussman J, Aoki K, Gottardi G (1988) Nomenclature of pyroxenes. Am Mineral 73:1123-1133

Nasution A, Haerani N, Mulyadi D, Hendrasto M (2004) Geological map of Agung volcano, Bali. Directorate of Volcanology and Geological Hazard Mitigation, Indonesia.

Newhall CG, Bronto S, Alloway B, Banks NG, Bahar I, del Marmol MA, Hadisantono RD, Holcomb RT, McGeehin J, Miksic JN, Rubin M, Sayudi SD, Sukhyar R, Andreastuti S, Tilling RI, Torley R, Trimble D, Wirakusumah AD (2000) 10,000 Years of explosive eruptions of Merapi Volcano, Central Java: archaeological and modern implications. J Volcanol Geotherm Res 100:9-50

Newhall CG, Self S (1982) The Volcanic Explosivity Index (VEI): An estimate of explosive magnitude for historical volcanism. J Geophys Res 87-C2:1231-1238

Peccerillo A, Taylor SR (1976) Geochemistry of Eocene calc-alkaline volcanic rocks from the Kastamonu area, Northern Turkey. Contrib Mineral Petrol 58:63-81

Piip BI, Suyehiro S, Tonani F (1963) Report of the UNESCO volcanological mission to study the Agung volcano. UNESCO, 65 pp.

Preece K, Barclay J, Gertisser R, Herd RA (2013) Textural and micro-petrological variations in the eruptive products of the 2006 dome-forming eruption of Merapi volcano, Indonesia: Implications for sub-surface processes. J Volcanol Geotherm Res 261:98-120

Purbo-Hadiwidjojo HM (1971) Geological Map Bali, Scale 1:250.000, Geological Survey of Indonesia.

Putirka KD (2008) Thermometers and barometers for volcanic systems. Rev Mineral Geochem 69:61-120

Pyle DM (2000) Sizes of volcanic eruptions. In: Sigurdsson H, Houghton B, Rymer H, Stix J, McNutt SR (eds) Encyclopedia of Volcanoes. Academic Press, pp 263-269

Rampino MR, Self S (1982) Historic eruptions of Tambora (1815) Krakatau (1883), and Agung (1963), their stratospheric aerosols, and climatic impact. Quat Res 18:127-143

Reimer PJ, Bard E, Bayliss A, Beck JW, Blackwell PG, Bronk Ramsey C, Buck CE, Cheng H, Edwards RL, Friedrich M, Grootes PM, Guilderson TP, Haflidason H, Hajdas I, Hatté C, Heaton TJ, Hoffmann DL, Hogg AG, Hughen KA, Kaiser KF, Kromer B, Manning SW, Niu M, Reimer RW, Richards DA, Scott EM, Southon JR, Staff RA, Turney CSM, van der Plicht J (2013) IntCal13 and Marine13 radiocarbon age calibration curves 0-50,000 years cal BP. Radiocarbon 55:1869-1887

Reubi O, Nicholls IA (2004a) Variability in eruptive dynamics associated with caldera collapse: an example from two successive eruptions at Batur volcanic field, Bali, Indonesia. Bull Volcanol 66:134-148

Reubi O, Nicholls IA (2004b) Magmatic evolution at Batur volcanic field, Bali, Indonesia: petrological evidence for polybaric fractional crystallization and implications for caldera-forming eruptions. J Volcanol Geotherm Res 138:345-369

Reubi O, Nicholls IA (2005) Structure and Dynamics of a Silicic Magmatic System Associated with Caldera-Forming Eruptions at Batur Volcanic Field, Bali, Indonesia. J Petrol 46:1367-1391

Ryu S, Kitagawa H, Nakamura E, Itaya T, Watanabe K (2013) K–Ar analyses of the post-caldera lavas of Bratan volcano in Bali Island, Indonesia — Ar isotope mass fractionation to light isotope enrichment. J Volcanol Geotherm Res 264:107-116

Self S, King AJ (1996) Petrology and sulphur and chlorine emissions of the 1963 eruption of Gunung Agung, Bali, Indonesia. Bull Volcanol 58:263-285

Self S, Rampino M (2012) The 1963–1964 eruption of Agung volcano (Bali, Indonesia). Bull Volcanol 74:1521-1536

Self S, Rampino MR, Barbera JJ (1981) The possible effects of large 19th and 20th century volcanic eruptions on zonal and hemispheric surface temperatures. J Volcanol Geotherm Res 11:41-60

Siebert L, Simkin T, Kimberly P (2010). Volcanoes of the World. Third edition. University of California Press, Berkeley

Sparks RSJ, Murphy MD, Lejeune AM, Watts RB, Barclay J, Young SR (2000) Control on the emplacement of the andesite lava dome of the Soufriere Hills volcano, Montserrat by degassing-induced crystallization. Terra Nova 12:14-20

Sutawidjaja I (2009) Ignimbrite Analyses of Batur Caldera, Bali, based on 14C dating. Jurnal Geologi Indonesia 4:189-202

Tanguy J-C, Ribière Ch, Scarth A, Tjeptjep WS (1998) Victims from volcanic eruptions: a revised database. Bull Volcanol 60:137-144

Turner MB, Cronin SJ, Stewart RB, Bebbington M, Smith IEM (2008) Using titanomagnetite textures to elucidate volcanic eruption histories. Geology 36:31-34

Van Daele M, Moernaut J, Silversmit G, Schmidt S, Fontijn K, Heirman K, Vandoorne W, De Clercq M, Van Acker J, Wolff C, Pino M, Urrutia R, Roberts SJ, Vincze L, De Batist M (2014) The 600 yr eruptive history of Villarrica Volcano (Chile) revealed by annually laminated lake sediments. Geol Soc Am Bull 126:481-498

Voight B, Constantine EK, Siswowidjoyo S, Torley R (2000) Historical eruptions of Merapi Volcano, Central Java, Indonesia, 1768–1998. J Volcanol Geotherm Res 100:69-138

Wigley TML, Ammann CM, Santer BD, Raper SCB (2005) Effect of climate sensitivity on the response to volcanic forcing. J Geophys Res: Atmos 110:D09107

Zen MT, Hadikusumo D (1964) Preliminary report on the 1963 eruption of Mt. Agung in Bali (Indonesia). Bull Volcanol 27:269-299

Zollinger H (1845) Een uitstapje naar het eiland Bali. Tijdschrift voor Nederlands Indie, jaargang 7, IV, pp 43 (in Dutch).

Table captions

Table 1 Radiocarbon dates of palaeosols between (scoria) fall deposits and charcoal entrained in PDC deposits. Samples are grouped by section (Fig 3), separated by grey horizontal bars. Analysis was performed at Beta Analytic Inc. (Florida, USA), either by conventional radiometric or AMS (Accelerator Mass Spectrometry) methods. Dates were calibrated using the IntCal13 calibration curve (Reimer et al. 2013) in OxCal 4.2 (Bronk Ramsey 2009). Calibrated ages reported at the 95.4% probability range. Samples are listed in stratigraphic order for each (composite) section, with the stratigraphically youngest sample on top. "Stratigraphic Unit" column indicates relation to immediately underlying, immediately overlying or enclosing deposits which were analysed for bulk geochemical composition (Supplementary Table 1, Fig 2).

Supplementary Table 1 Bulk geochemical data obtained by ICP-OES (major elements, Sc, V) and ICP-MS (trace elements) at Activation Laboratories Ltd., Ontario, Canada. Fe_2O_3* reported as total iron. PDC: pyroclastic density current deposit, BAF: block-and-ash flow deposit.

Supplementary Table 2a Plagioclase compositions analysed by EMP. Where possible, multiple analyses were run per crystal (each given a number), e.g. in core (c), rim (r) or intermediate (i) positions, as indicated in the analysis name. "Trav" refers to regularly spaced analyses from core to rim. Analyses of intermediate positions were taken as core analyses in Figure 9. For sample details, see Figure 2 and Supplementary Table 1.

Supplementary Table 2b Pyroxene compositions analysed by EMP. Where possible, multiple analyses were run per crystal (each given a number), e.g. in core (c), rim (r) or intermediate (i) positions, as indicated in the analysis name. "Trav" refers to regularly spaced

analyses from core to rim. Analyses of intermediate positions were taken as core analyses in Figure 10. For sample details, see Figure 2 and Supplementary Table 1. Cpx-opx pairs refer to touching pairs which were used for temperature calculations.

Supplementary Table 2c Olivine compositions analysed by EMP. Where possible, multiple analyses were run per crystal (each given a number), e.g. in core (c), rim (r) or intermediate (i) positions, as indicated in the analysis name. For sample details, see Figure 2 and Supplementary Table 1.

Supplementary Table 2d Magnetite compositions analysed by EMP.

Supplementary Table 2e Melt inclusion compositions in pyroxenes and olivine analysed by EMP. Host mineral is indicated in analysis name.

Figure captions

Fig 1 SRTM DEM at 3 arcsecond (~90 m) resolution (Jarvis et al. 2008) of east Bali showing the two active volcanoes, Gunung Batur and Gunung Agung. Gunung Seraja is considered inactive and of Lower Pleistocene age (Purbo-Hadiwidjojo 1971). Black stars indicate visited outcrops. Named outcrops refer to stratigraphic columns in Figure 3.

Fig 2 Representative photos of outcrops. Samples taken for chemistry in yellow, for radiocarbon dating (red stars) in blue. See Figure 3, Table 1 and Supplementary Table 1.

Fig 3 Schematic logs of the most complete stratigraphic sections. The sections west of Agung represent Agung's history of eruptions generating tephra fall deposits in approximately the last 3-5 ky. The sections S and SE of Agung show a history of repeated PDCs in approximately the last 1 ky. Correlations are suggested and units named where possible, but are hampered by the repetitive, dominantly basaltic andesitic bulk composition of the deposits. Diamonds indicate bulk SiO_2 content; those delineated in black represent samples for which we acquired mineral compositional data. A useful marker horizon is the 1257AD pumice fall deposit from Samalas (Lavigne et al. 2013). Radiocarbon ages are given as the mean and standard deviation of the calibrated range at the 95.4% probability range (Table 1). Sample names refer to those samples for which analyses are available, either radiocarbon dating (black, Table 1) or bulk geochemistry (grey, Supplementary Table 1). For brevity, "AG0" was omitted from the sample name.

Fig 4 K_2O–SiO_2 classification diagram (Peccerillo and Taylor 1976). Individual data points represent bulk analyses of Agung rocks, Batur and Samalas 1257AD pumice. Some Agung

1963AD data after Self and King (1996). Melt inclusion (MI) data represent EMP point analyses of MI in pyroxene or olivine in Agung scoria fall samples. Compositional fields for Batur (Reubi and Nicholls 2004b, 2005), Rinjani (Foden 1983), Bratan (Ryu et al. 2013) and Merapi (Costa et al. 2013; Gertisser and Keller 2003a; Preece et al. 2013) given for reference. Two separate Merapi fields represent medium- and high-K series, typically the older (> 1.9 ka) and younger (<1.9 ka) Merapi deposits respectively, as defined by Gertisser and Keller (2003a).

Fig 5 Spatial distribution of 1963AD and 1843AD deposits, suggesting similar magnitudes for both events. Base map data from Jarvis et al (2008), 500 m contour intervals. Volcano names other than Agung given for reference. Isopach contours of 1963AD fall deposit (units 1–3, corresponding to first explosions and paroxysmal phase of 17th March) after Self and Rampino (2012); 1963 lava flow (Al14), PDC (Aap6) and lahar (Alh3) deposits after Nasution et al. (2004). We interpret Al13 (lava flow), Ajp1 (tephra fall) and Aap5 (PDC) units defined by Nasution et al. (2004) to correspond to the 1843AD eruption, of which we identified deposits on all flanks of the volcano.

Fig 6 Selected trace element variation diagrams for Agung and Batur. **(a)** Zr/Nb vs. Nb; **(b)** Ce vs. Nb. Individual points represent bulk analyses of Agung, Batur and 1257AD Samalas samples. Some Agung 1963AD data after Self and King (1996). RN04: Reubi and Nicholls (2004b), RN05: Reubi and Nicholls (2005). Grey arrows indicate fractional crystallisation paths modelled with Igpet (Carr 2012) using appropriate partition coefficients from the GERM database (http://earthref.org/KDD/), suggesting clear source differences between both volcanoes.

Fig 7 Selection of optical microscope images taken under cross-polarised light: **(a)** Sample AG012I, representing the 1963AD scoria fall deposit; **(b)** Sample AG001bisB, representing a basaltic – basaltic andesitic PDC deposit which occurs under the 1257AD Samalas deposit (Fig 3), and with a variety of plagioclase textures; **(c)** Sample AG001bisE, representing a basaltic andesitic PDC deposit above the 1257AD Samalas deposit (Fig 3) and with a lighter-coloured inclusion in a darker groundmass; **(d)** Sample AG012E, representing the 1843AD PDC deposits of andesitic composition, with dominantly a relatively light-coloured groundmass and few sieve-textured plagioclase.

Fig 8 Selection of backscatter electron images of mineral phases analysed by EMP (Supplementary Table 2). White X: approximate locations of analysed points. **(a)** Sample AG042B (1843AD), plagioclase 24, with calcic sieve-textured core: core An_{87-89}, rim An_{67}; **(b)** Sample AG042I, plagioclase 13 showing complex zoning with An content ranging from 42 to 70% (higher An values are lighter grey); **(c)** Sample AG042B, pyroxene pair 20 (clinopyroxene left, orthopyroxene right); **(d)** Sample AG042I, clinopyroxene 11 with large core (Mg# = 74-75), broad intermediate zone (Mg# = 86), and narrow outer rim (Mg# = 79); **(e)** Sample AG042I, olivine 1 (Fo_{80-75}) with orthopyroxene rim; **(f)** Sample AG042I, subhedral olivine 6 (left, Fo_{80-79}) and 7 (right, Fo_{80}).

Fig 9 Histograms of plagioclase core and rim An composition, grouped by deposit type and host rock composition. Less evolved samples (<55% SiO_2) show a more restricted range of plagioclase core compositions than more evolved samples (≥55% SiO_2), and tend to have high-calcic cores.

Fig 10 Histograms of pyroxene core and rim Mg#, grouped by host rock composition. Both clino- and orthopyroxene generally show very little variation between core and rim composition. Only in the more evolved samples, especially of PDC deposits, orthopyroxene rims tend to be more Mg-rich than cores.

Fig 11 Cumulative deposit volume versus time plot of Late Holocene Agung pyroclastic eruptions. Eruption ages are approximate, assuming a constant eruptive frequency of 1 event per century (52 events in ~5.2 ky; Fig 3). Eruption volumes are estimated by assigning a VEI to each recognised event, relative to the well-characterised 1963AD eruption (VEI 4). Main eruptions are highlighted (sample names/compositions: Fig 3, Supplementary Table 1). See text for further details.

Figure 1

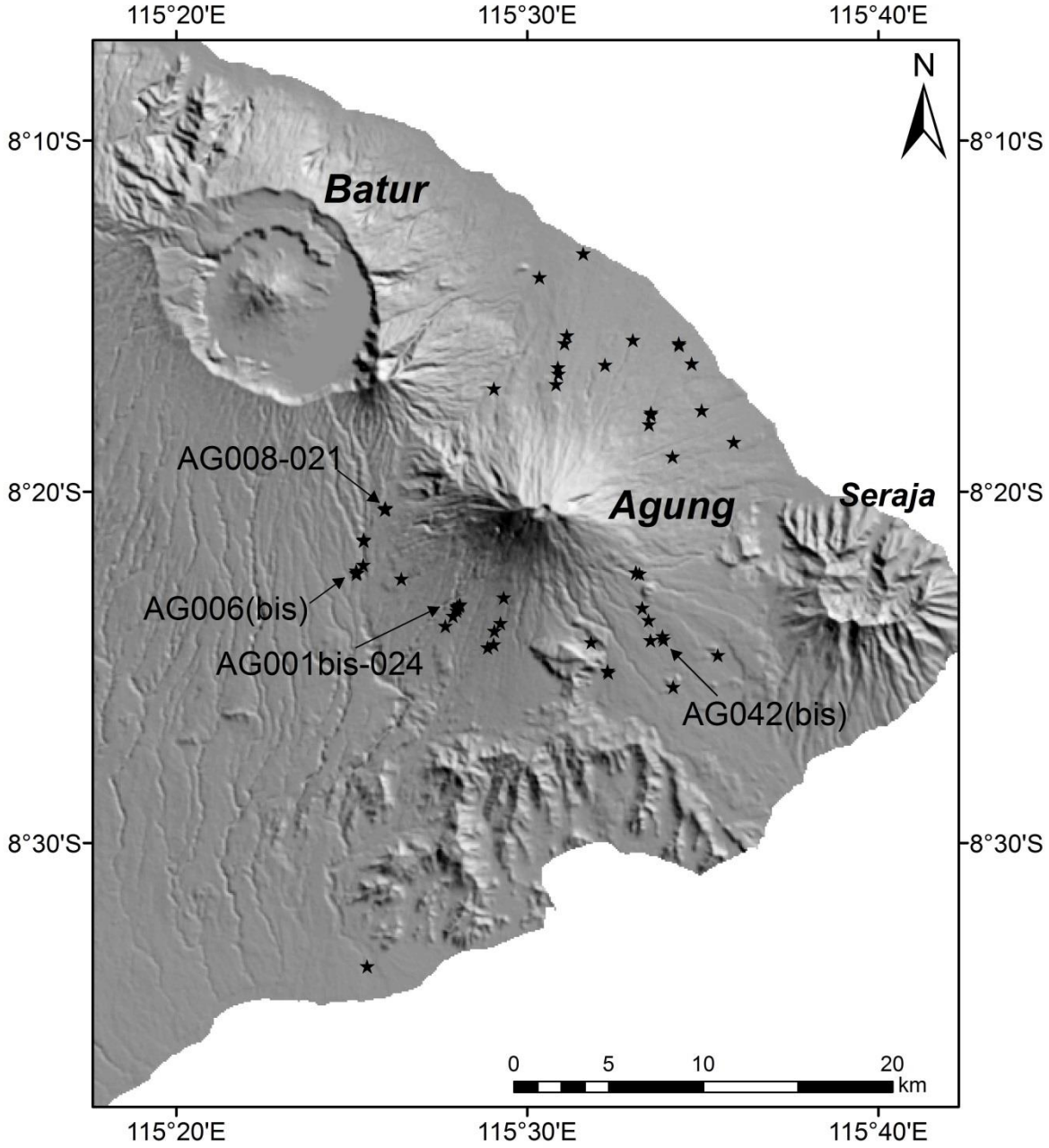
115°20'E
115°30'E
115°40'E
N
8°10'S
8°20'S
8°30'S
Batur
Agung
Seraja
AG008-021
AG006(bis)
AG001bis-024
AG042(bis)
0
5
10
20
km

Figure 2

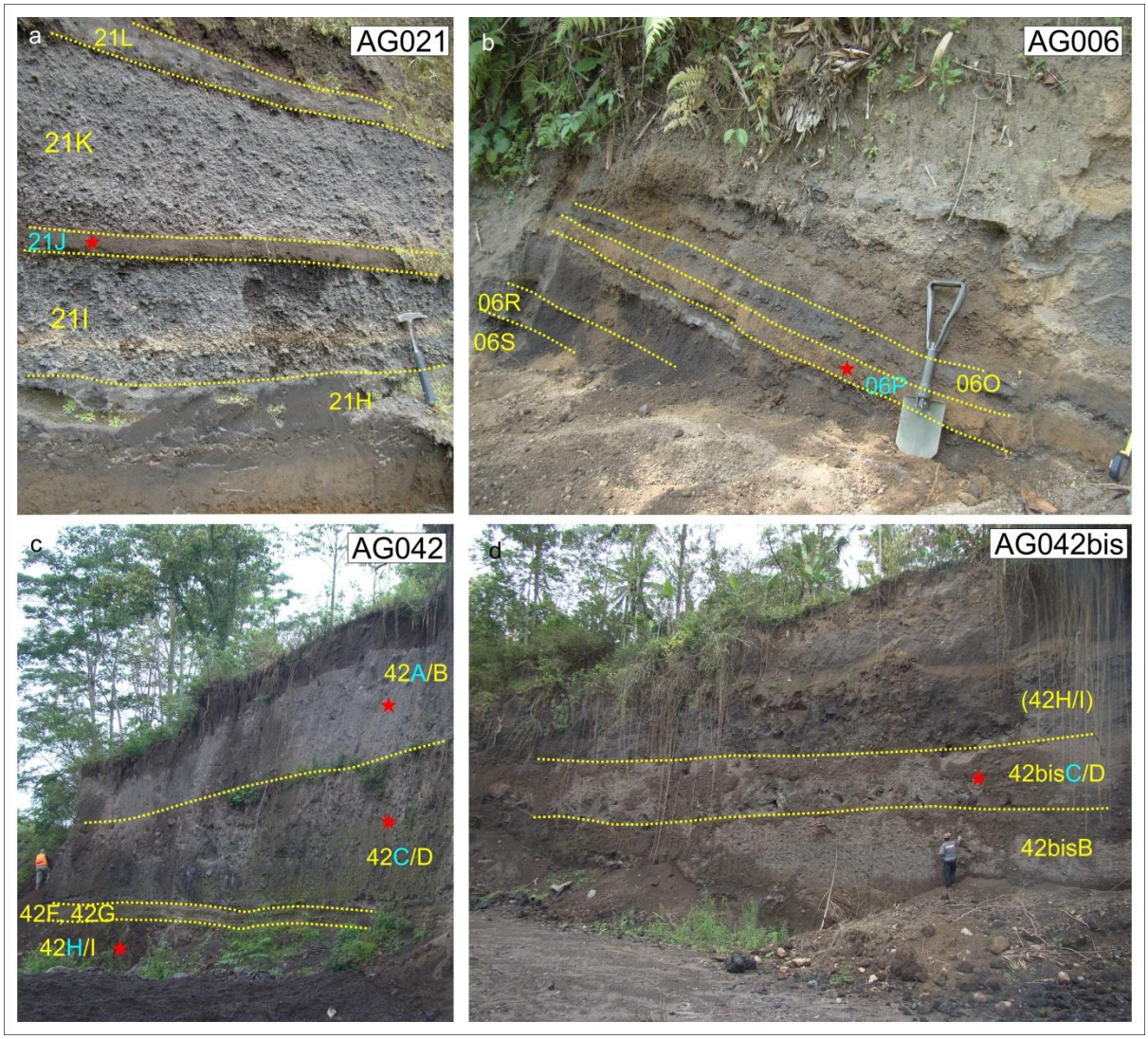
a
AG021
21L
21K
21J
21I
21H
b
AG006
06R
06S
06P
06O
c
AG042
42A/B
42C/D
42F, 42G
42H/I
d
AG042bis
(42H/I)
42bisC/D
42bisB

Figure 3

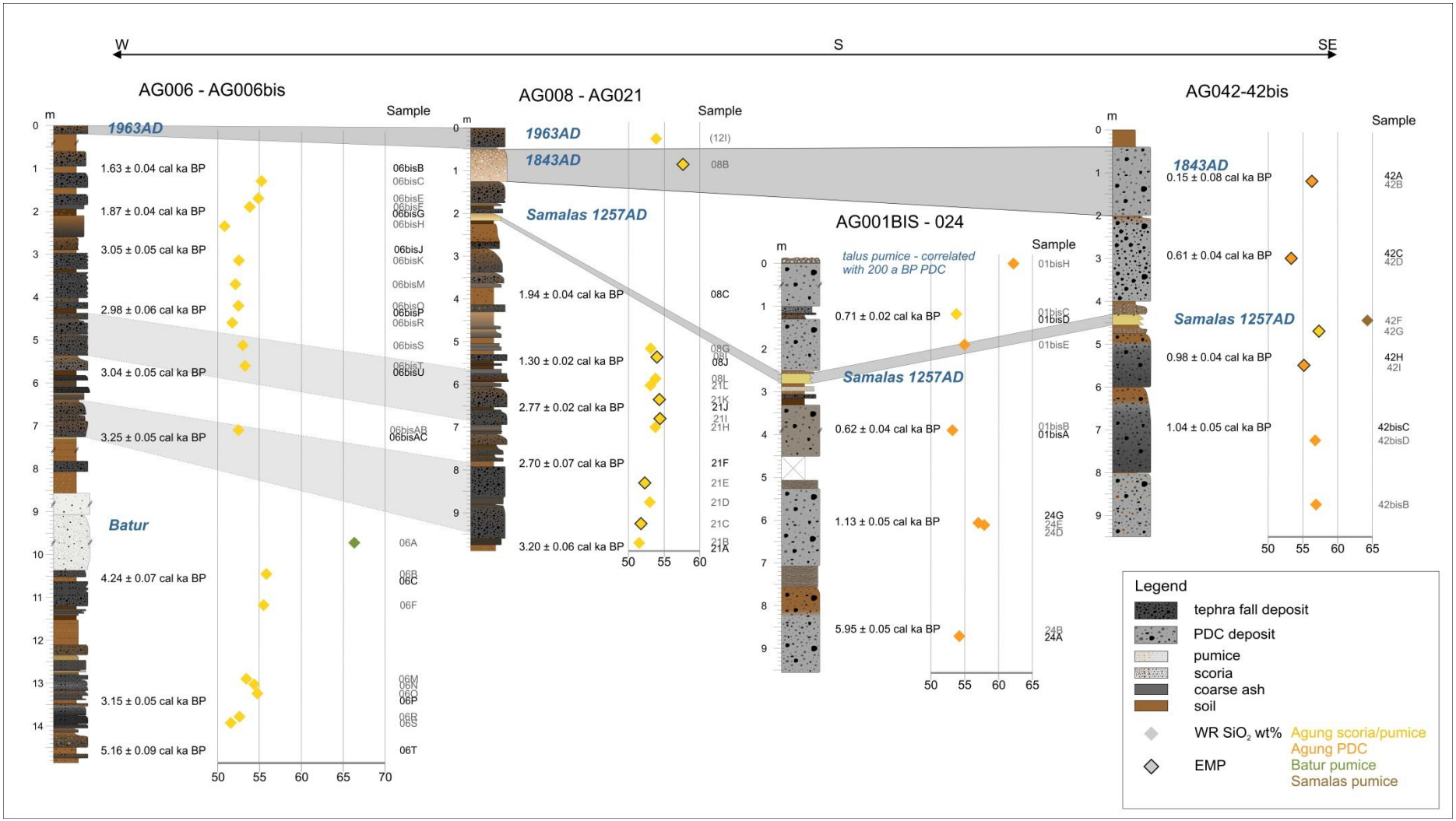
W
S
SE
AG006 - AG006bis
AG008 - AG021
AG001BIS - 024
AG042-42bis
m
Sample
1963AD
1843AD
Samalas 1257AD
Batur
1.63 ± 0.04 cal ka BP
1.87 ± 0.04 cal ka BP
3.05 ± 0.05 cal ka BP
2.98 ± 0.06 cal ka BP
3.04 ± 0.05 cal ka BP
3.25 ± 0.05 cal ka BP
4.24 ± 0.07 cal ka BP
3.15 ± 0.05 cal ka BP
5.16 ± 0.09 cal ka BP
1.94 ± 0.04 cal ka BP
1.30 ± 0.02 cal ka BP
2.77 ± 0.02 cal ka BP
2.70 ± 0.07 cal ka BP
3.20 ± 0.06 cal ka BP
talus pumice - correlated with 200 a BP PDC
0.71 ± 0.02 cal ka BP
0.62 ± 0.04 cal ka BP
1.13 ± 0.05 cal ka BP
5.95 ± 0.05 cal ka BP
0.15 ± 0.08 cal ka BP
0.61 ± 0.04 cal ka BP
0.98 ± 0.04 cal ka BP
1.04 ± 0.05 cal ka BP
Legend
tephra fall deposit
PDC deposit
pumice
scoria
coarse ash
soil
WR SiO2 wt%
EMP
Agung scoria/pumice
Agung PDC
Batur pumice
Samalas pumice

Figure 4

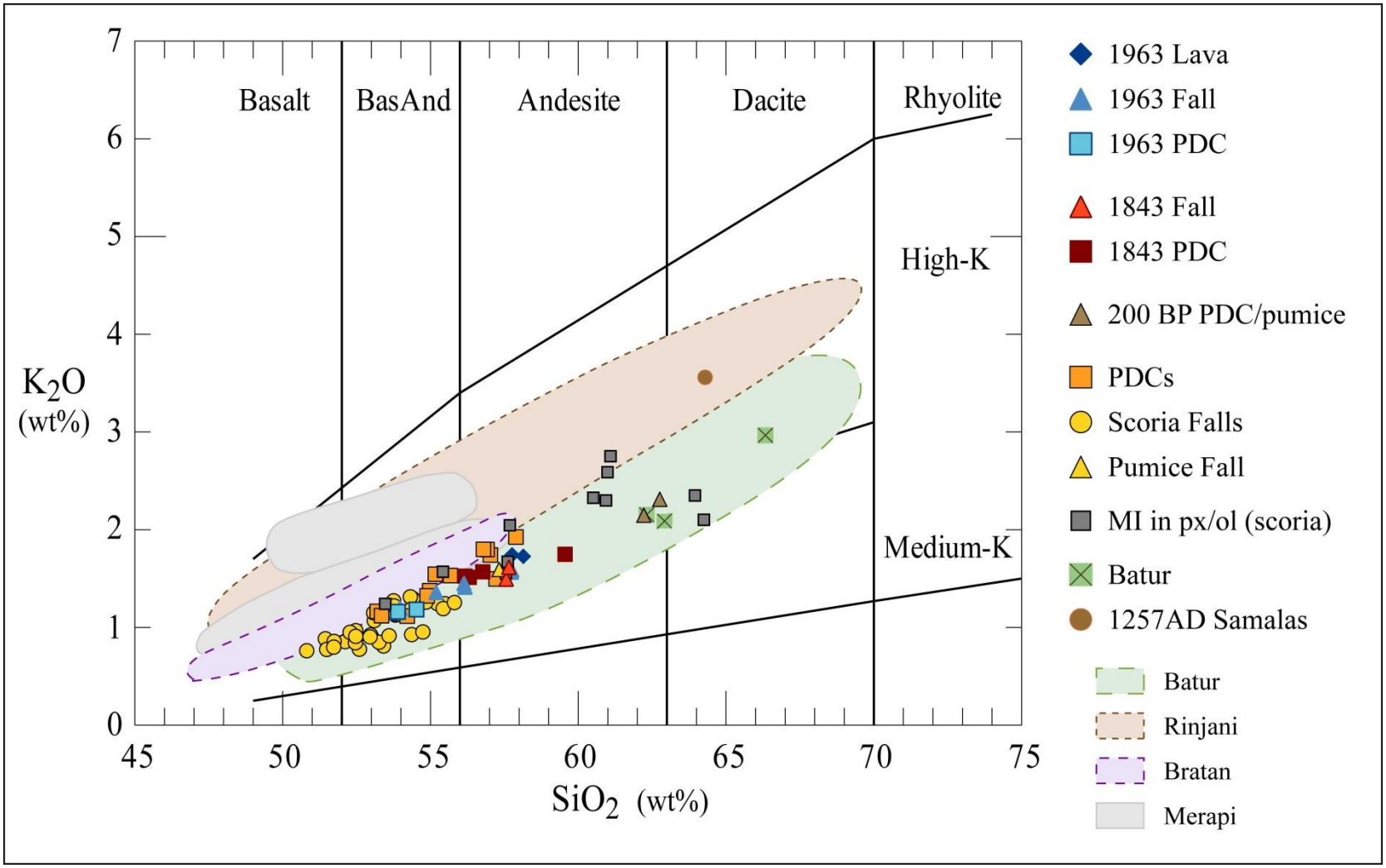
Basalt
BasAnd
Andesite
Dacite
Rhyolite
High-K
Medium-K
K_2O (wt%)
SiO_2 (wt%)
0
1
2
3
4
5
6
7
45
50
55
60
65
70
75
1963 Lava
1963 Fall
1963 PDC
1843 Fall
1843 PDC
200 BP PDC/pumice
PDCs
Scoria Falls
Pumice Fall
MI in px/ol (scoria)
Batur
1257AD Samalas
Batur
Rinjani
Bratan
Merapi

Figure 5

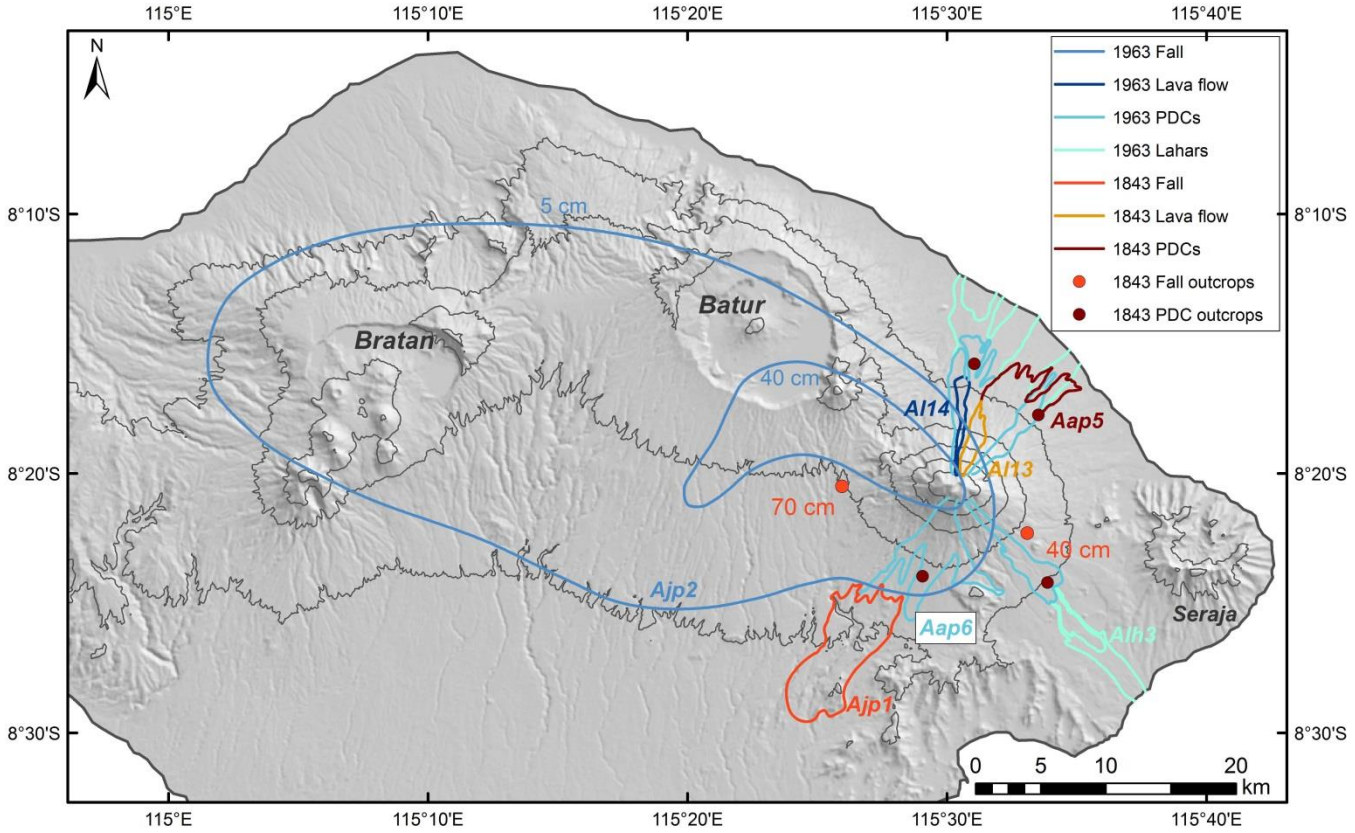
115°E
115°10'E
115°20'E
115°30'E
115°40'E
N
8°10'S
8°20'S
8°30'S
1963 Fall
1963 Lava flow
1963 PDCs
1963 Lahars
1843 Fall
1843 Lava flow
1843 PDCs
1843 Fall outcrops
1843 PDC outcrops
5 cm
40 cm
70 cm
40 cm
Batur
Bratan
Seraja
Al14
Aap5
Al13
Ajp2
Aap6
Alh3
Ajp1
0 5 10 20
km

Figure 6

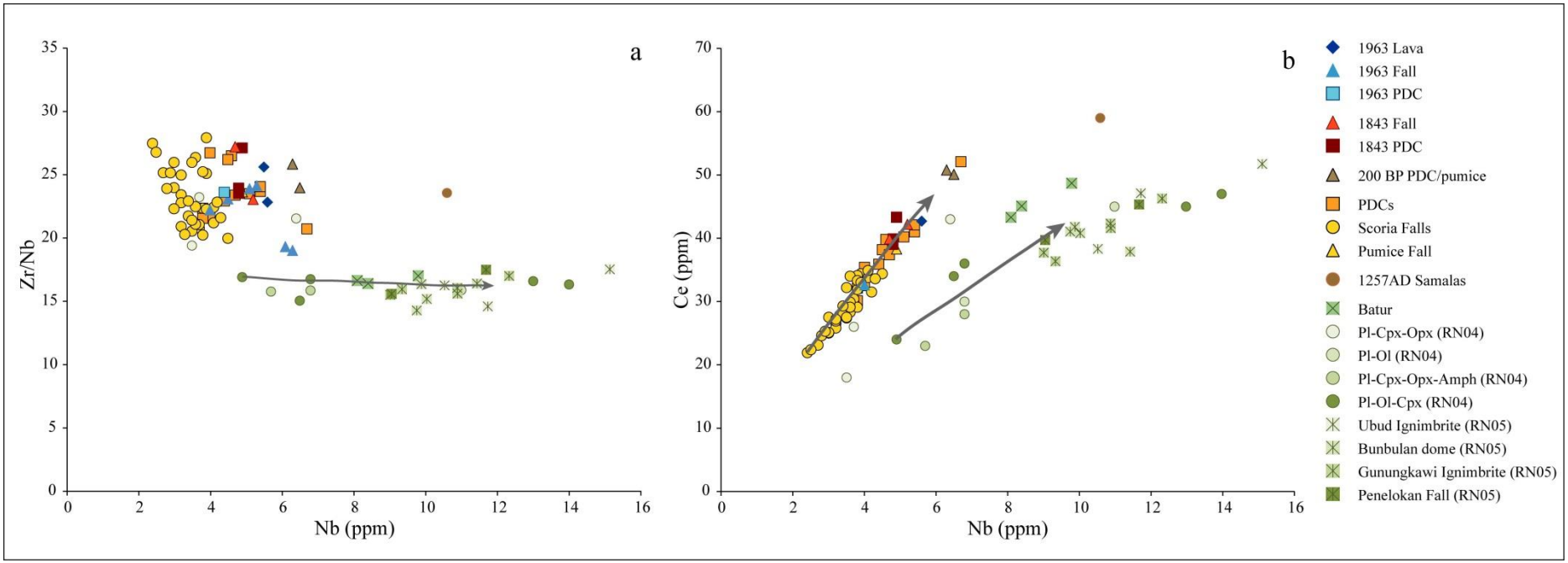
a
Zr/Nb
Nb (ppm)
b
Ce (ppm)
Nb (ppm)
1963 Lava
1963 Fall
1963 PDC
1843 Fall
1843 PDC
200 BP PDC/pumice
PDCs
Scoria Falls
Pumice Fall
1257AD Samalas
Batur
Pl-Cpx-Opx (RN04)
Pl-Ol (RN04)
Pl-Cpx-Opx-Amph (RN04)
Pl-Ol-Cpx (RN04)
Ubud Ignimbrite (RN05)
Bunbulan dome (RN05)
Gunungkawi Ignimbrite (RN05)
Penelokan Fall (RN05)

Figure 7

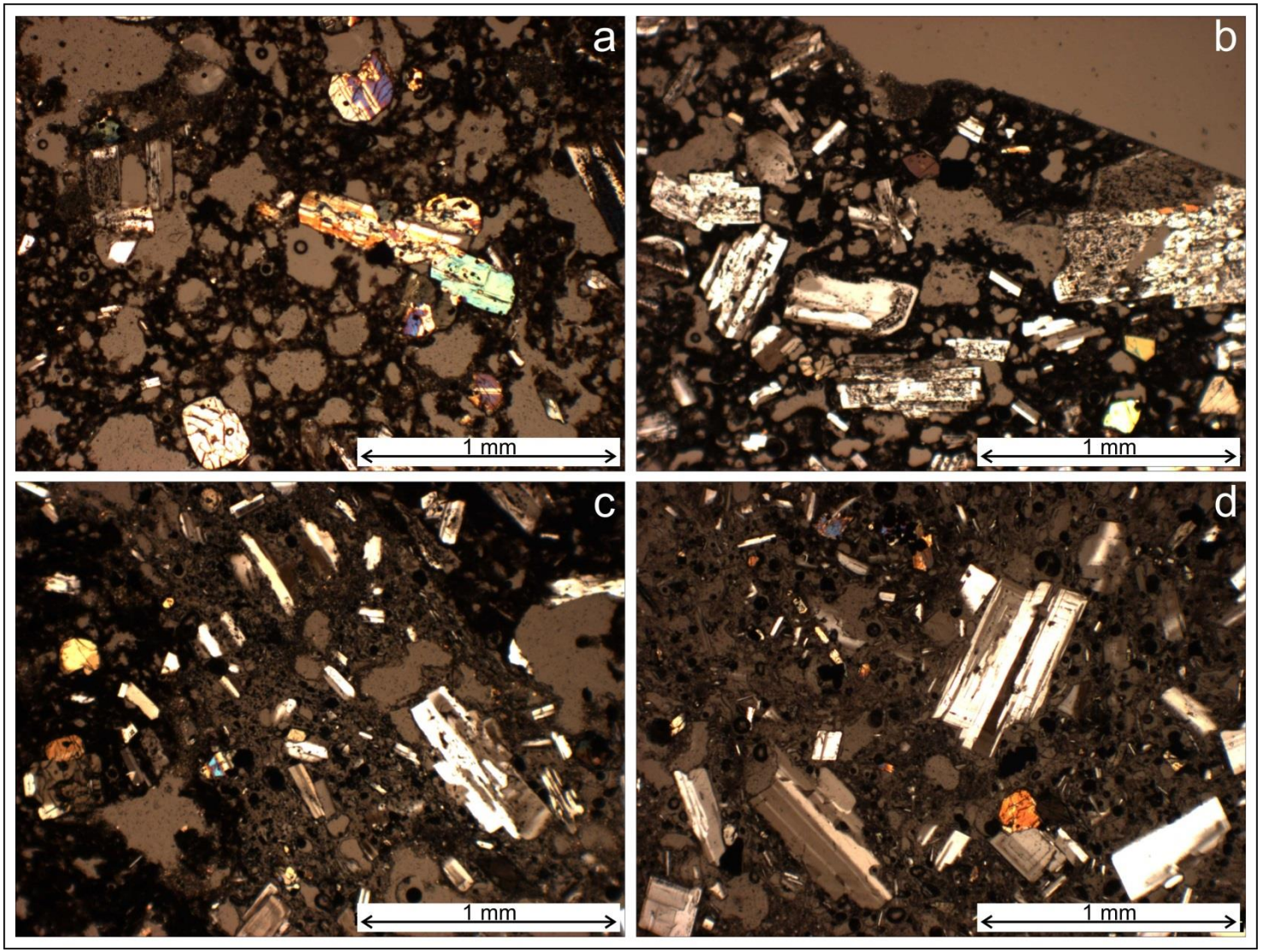

Figure 8

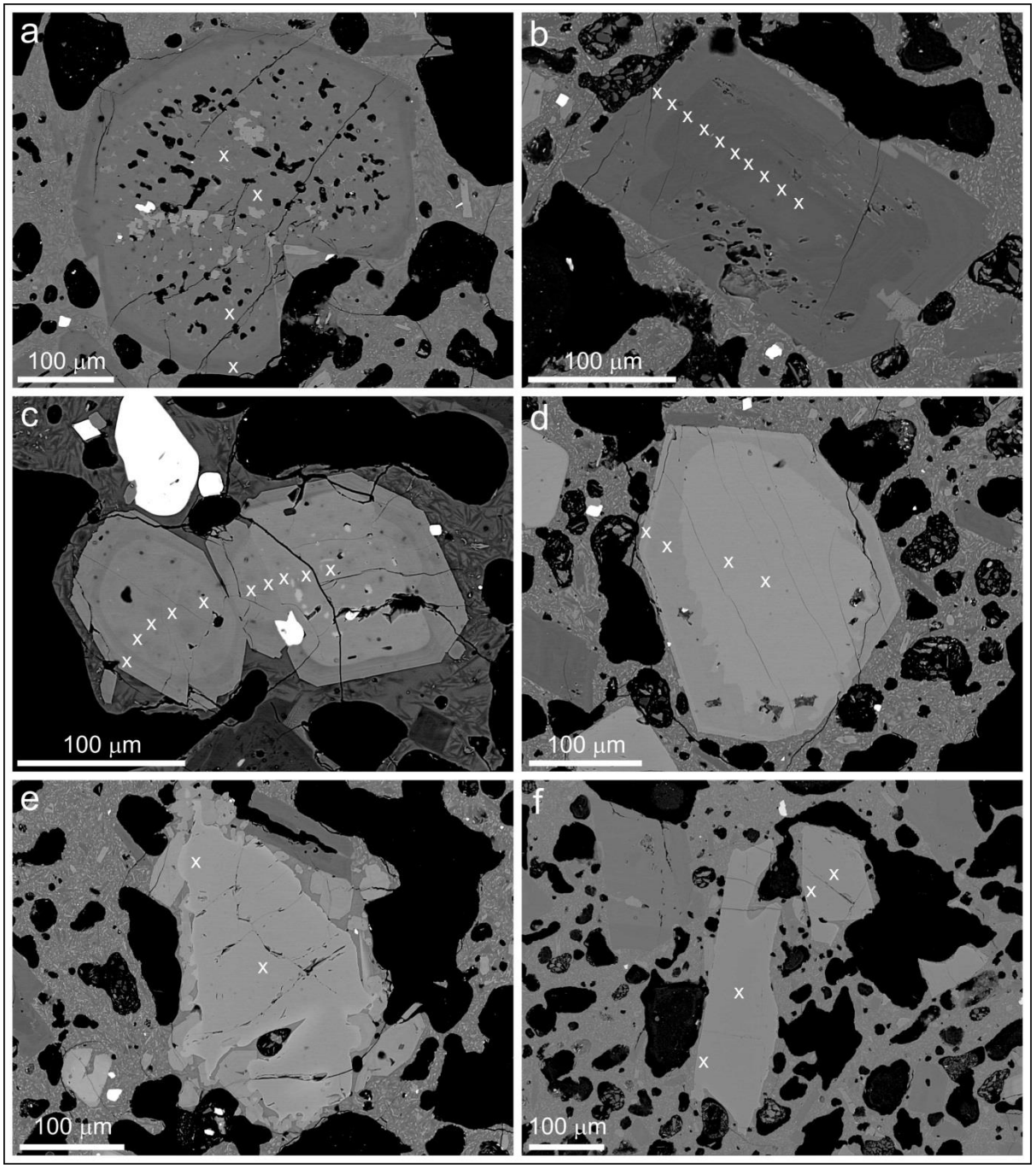

Figure 9

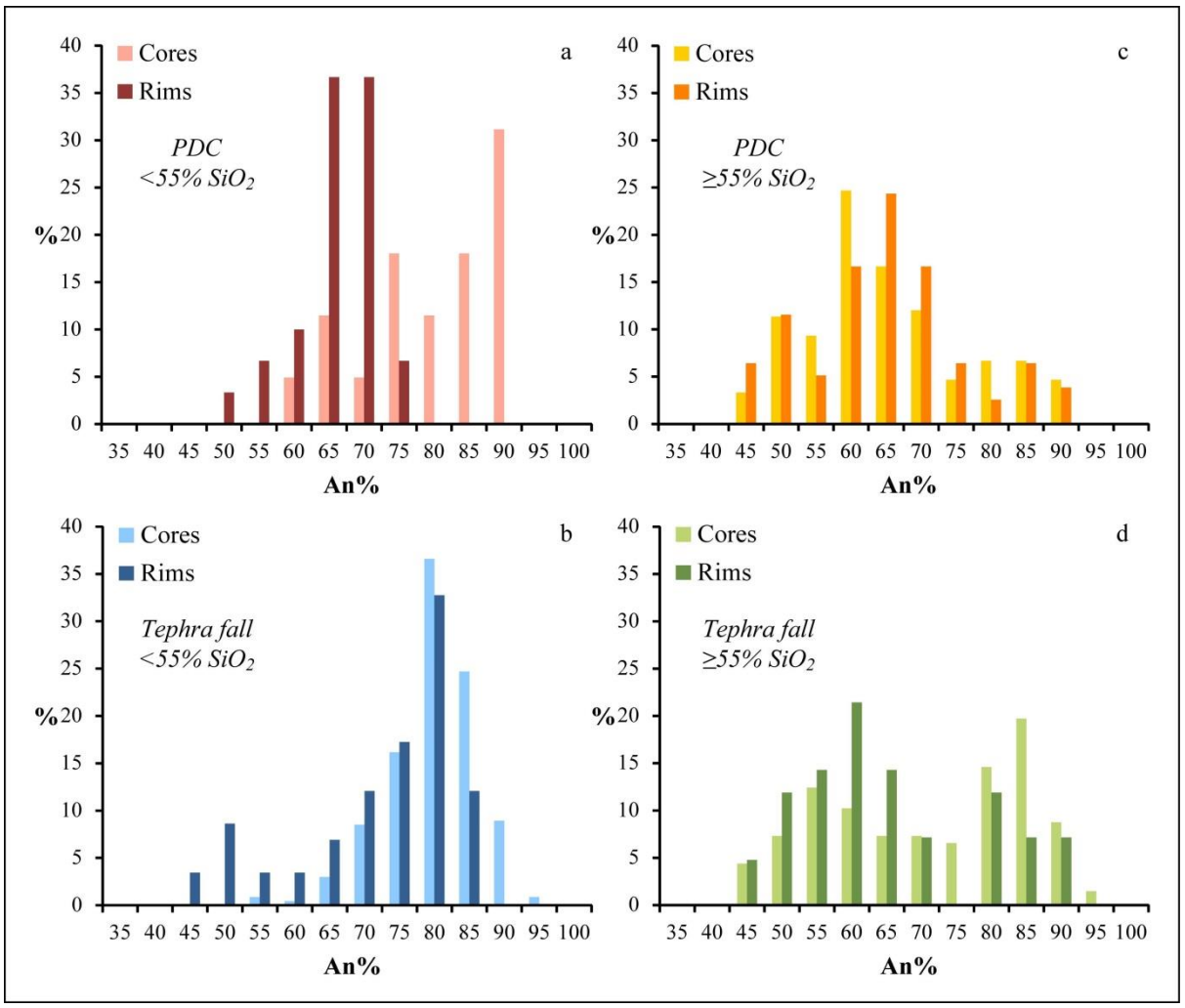
a
Cores
Rims
PDC
<55% SiO2
c
Cores
Rims
PDC
≥55% SiO2
b
Cores
Rims
Tephra fall
<55% SiO2
d
Cores
Rims
Tephra fall
≥55% SiO2
%
An%
0 5 10 15 20 25 30 35 40
35 40 45 50 55 60 65 70 75 80 85 90 95 100

Figure 10

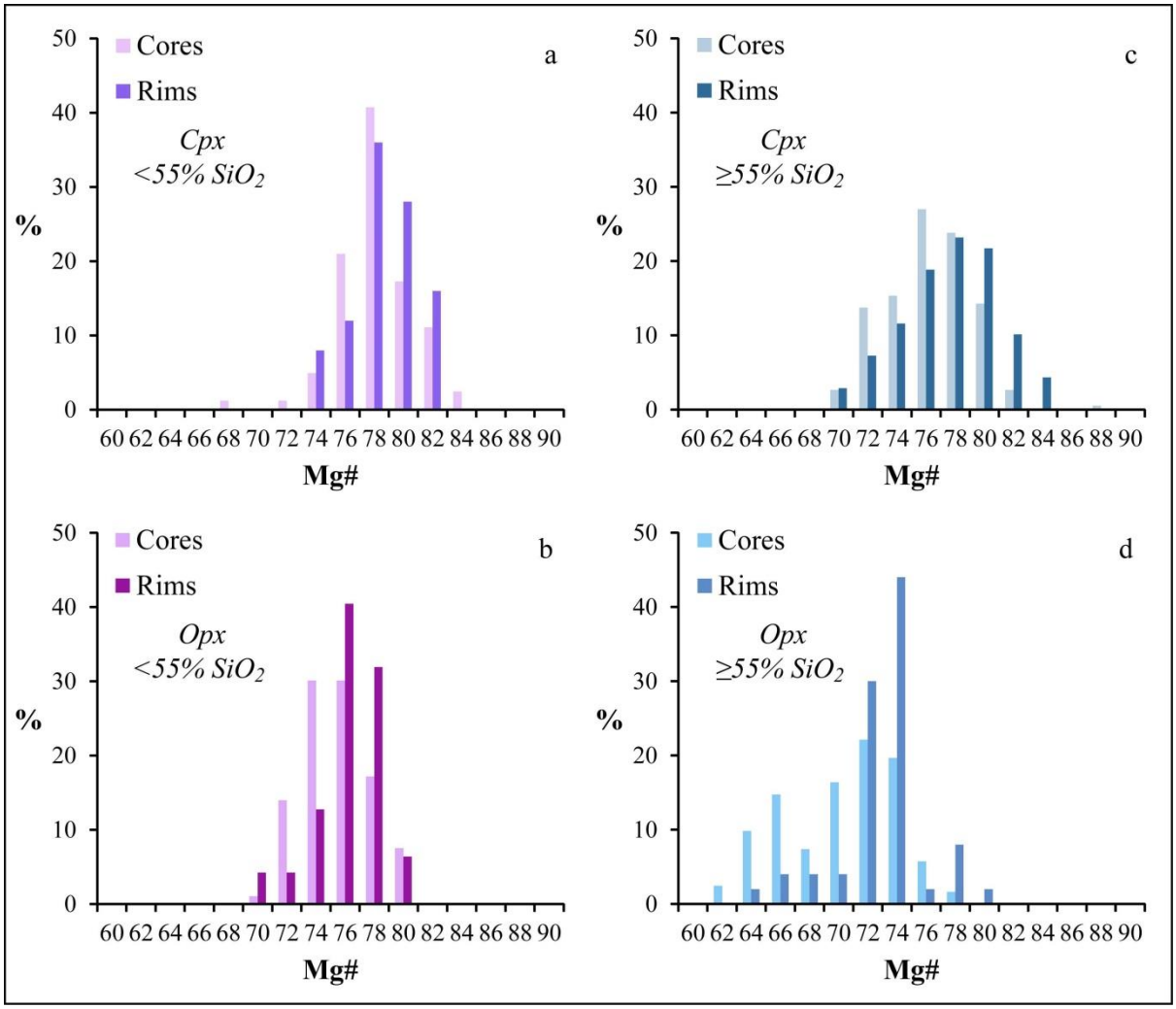
a
Cores
Rims
Cpx
<55% SiO2
%
Mg#
c
Cores
Rims
Cpx
≥55% SiO2
%
Mg#
b
Cores
Rims
Opx
<55% SiO2
%
Mg#
d
Cores
Rims
Opx
≥55% SiO2
%
Mg#

Figure 11

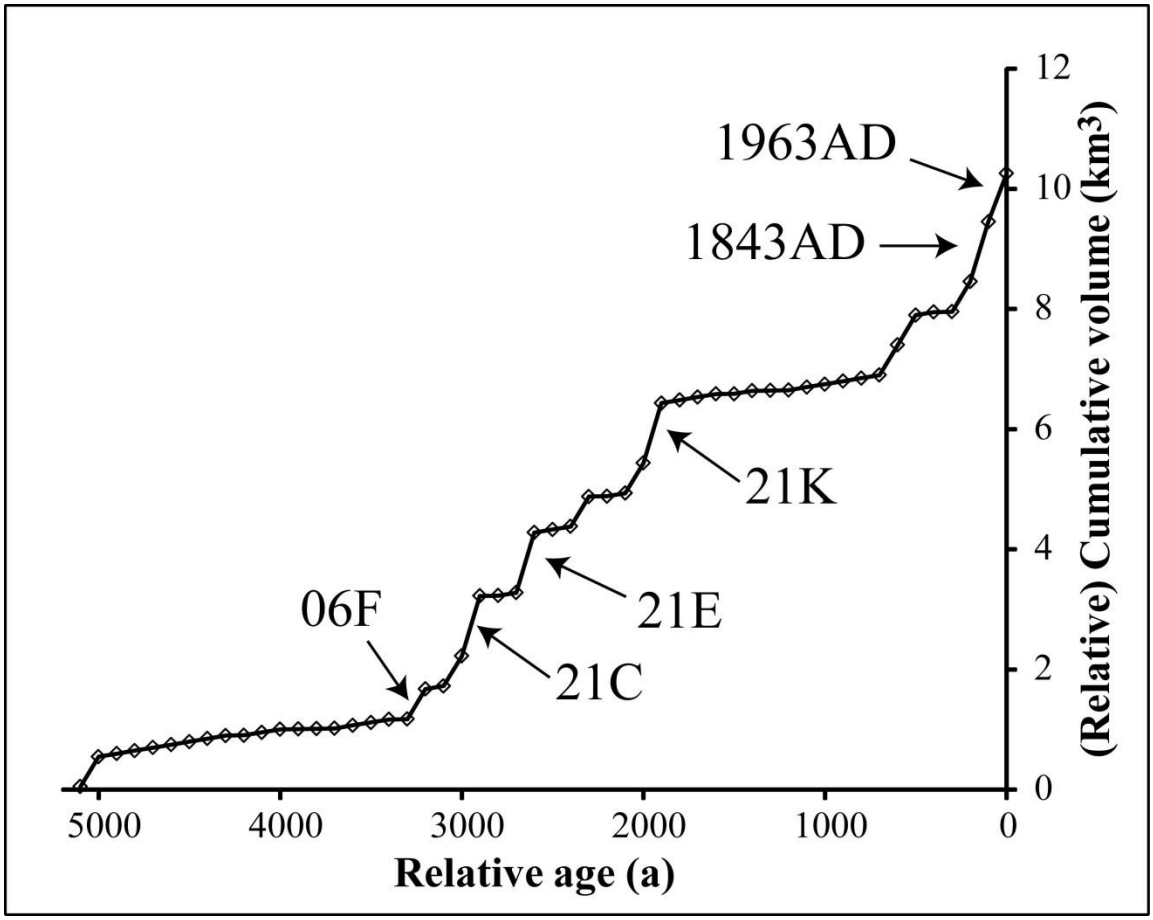
1963AD
1843AD
21K
21E
21C
06F
(Relative) Cumulative volume (km³)
Relative age (a)
0
2
4
6
8
10
12
5000
4000
3000
2000
1000
0

Sample	Beta lab code	Method	Material	Pre-treatment	Date (a BP, 1σ)	δ ^{13}C	Cal. a BP (95.4%)	Cal. ka BP (μ ± σ; 95.4%)	Stratigraphic Unit
AG001bisD	310663	AMS	charred wood	acid/alkali/acid	790 ± 30	-27.1	672 – 760	0.71 ± 0.02	Scoria fall covering PDC (AG001bisE)
AG001bisA	310672	Radiometric	charcoal	acid/alkali/acid	670 ± 30	-24.6	559 – 600 (42.3%) 631 – 677 (53.1%)	0.62 ± 0.04	PDC (AG001bisB)
AG024G	310674	Radiometric	charcoal	acid/alkali/acid	1200 ± 30	-23.4	1010 – 1022 (1.4%) 1055 – 1185 (87.8%) 1206 – 1236 (6.2%)	1.13 ± 0.05	PDC (AG024D-E)
AG024A	310673	AMS	charcoal	acid washes	5190 ± 40	-23.1	5773 – 5780 (0.3%) 5795 – 5803 (0.4%) 5891 – 6018 (91.3%) 6081 – 6108 (2.3%) 6157 – 6172 (1.1%)	5.95 ± 0.05	PDC (AG024B)
AG006bisB	310665	AMS	palaeosol	acid washes	1720 ± 30	-23.8	1560 – 1703	1.63 ± 0.04	between scoria falls (above AG006bisC)
AG006bisG	309172	AMS	palaeosol	acid washes	1920 ± 30	-24.1	1746 – 1751 (0.3%) 1812 – 1948 (95.1%)	1.87 ± 0.04	between ash falls (AG006bisF-H)
AG006bisJ	309173	AMS	palaeosol	acid washes	2910 ± 30	-26.3	2960 – 3158	3.05 ± 0.05	between scoria falls (above AG006bisK)
AG006bisP	309174	AMS	palaeosol	acid washes	2860 ± 40	-24.5	2865 – 3078 (93.2%) 3095 – 3106 (1.2%) 3129 – 3138 (1.0%)	2.98 ± 0.06	between scoria falls (below AG006bisO)
AG006bisU	309175	AMS	palaeosol	acid washes	2900 ± 30	-24.5	2953 – 3083 (78.8%) 3090 – 3156 (16.6%)	3.04 ± 0.05	between scoria falls (below AG006bisT)
AG006bisAC	310664	AMS	palaeosol	acid washes	3040 ± 30	-26.4	3165 – 3346	3.25 ± 0.05	between scoria falls (below AG006bisAB)
AG006C	310666	AMS	palaeosol	acid washes	3830 ± 30	-26.0	4101 – 4113 (1.5%) 4147 – 4300 (81.4%) 4305 – 4317 (1.1%) 4324 – 4356 (6.2%) 4367 – 4405 (5.2%)	4.24 ± 0.07	underlying scoria fall (AG006B) and Batur pumice fall (AG006A)

AG006P	309176	AMS	palaeosol	acid washes	2980 ± 30	-24.2	3061 – 3246 (94.3%) 3308 – 3321 (1.1%)	3.15 ± 0.05	between ash falls (below AG006O)
AG006T	309177	AMS	palaeosol	acid washes	4480 ± 30	-23.4	4979 – 5008 (4.6%) 5036 – 5290 (90.8%)	5.16 ± 0.09	between scoria falls
AG008C	309178	AMS	palaeosol with charcoal	acid/alkali/acid	1990 ± 30	-25.0	1878 – 1998	1.94 ± 0.04	between scoria falls
AG008J	310667	AMS	palaeosol	acid washes	1380 ± 30	-25.7	1270 – 1344	1.30 ± 0.02	between scoria falls (below AG008I)
AG021J	310671	AMS	palaeosol	acid washes	2650 ± 30	-23.5	2740 – 2799 (89.5%) 2818 – 2844 (5.9%)	2.77 ± 0.02	between scoria falls (AG021K-I)
AG021F	310670	AMS	palaeosol	acid washes	2570 ± 30	-26.5	2508 – 2529 (2.5%) 2537 – 2590 (10.2%) 2616 – 2634 (5.2%) 2697 – 2758 (77.5%)	2.70 ± 0.07	between scoria falls (above AG021E)
AG021A	309180	AMS	palaeosol	acid washes	3010 ± 30	-24.4	3077 – 3096 (4.4%) 3106 – 3259 (78.9%) 3289 – 3335 (12.2%)	3.20 ± 0.06	underlying bottom ash fall (AG021B)
AG042A	310676	AMS	charcoal	acid/alkali/acid	150 ± 30	-26.3	… – 41 (17.7%) 60 – 154 (30.0%) 167 – 233 (31.4%) 241 – 284 (16.3%)	0.15 ± 0.08	PDC (AG042B; 1843 AD)
AG042C	310678	Radiometric	charcoal	acid/alkali/acid	650 ± 30	-26.0	556 – 607 (51.9%) 625 – 670 (43.5%)	0.61 ± 0.04	PDC (AG042D; block-and-ash flow)
AG042H	310679	AMS	charcoal	acid/alkali/acid	1070 ± 30	-24.5	929 – 1010 (74.5%) 1022 – 1055 (20.9%)	0.98 ± 0.04	PDC (AG042I)
AG042bisC	310677	Radiometric	charcoal	acid/alkali/acid	1130 ± 30	-25.1	962 – 1090 (86.6%) 1108 – 1145 (5.6%) 1159 – 1173 (3.2%)	1.04 ± 0.05	PDC (AG042bisD)
AG012D	309169	Radiometric	charred wood	acid/alkali/acid	110 ± 30	-25.9	12 – 148 (65.5%) 187 – 205 (2.8%) 211 – 270 (27.1%)	0.13 ± 0.08	PDC (AG012E; 1843AD)

AG017G	309170	Radiometric	charcoal	acid/alkali/acid	1140 ± 30	-25.7	969 – 1096 (78.6%) 1103 – 1149 (11.3%) 1158 – 1174 (5.5%)	1.05 ± 0.05	PDC
AG018E	309171	Radiometric	charred wood	acid/alkali/acid	123.0 ± 0.5 pMC	-13.9	*modern*	*modern*	PDC (possibly 1963 AD)
AG018D	309179	AMS	palaeosol	acid washes	103.5 ± 0.3 pMC	-13.0	*modern*	*modern*	between PDCs
AG020bisG	310669	AMS	palaeosol	acid washes	2450 ± 30	-26.2	2360 – 2544 (53.2%) 2558 – 2619 (15.5%) 2630 – 2703 (26.7%)	2.54 ± 0.10	between scoria fall (above, AG020bisF) and stream deposits (below)
AG20bisA	310668	AMS	palaeosol	acid washes	3850 ± 40	-25.2	4153 – 4410	4.27 ± 0.08	underlying scoria fall (AG020bisB)
AG028A	310675	Radiometric	charcoal	acid/alkali/acid	150 ± 30	-25.5	… – 41 (17.7%) 60 – 154 (30.0%) 167 – 233 (31.4%) 241 – 284 (16.3%)	0.15 ± 0.08	PDC (AG028B; 1843AD)
AG045E	310680	Radiometric	charcoal	acid/alkali/acid	200 ± 30	-26.0	… – 25 (19.3%) 140 – 222 (51.2%) 261 – 304 (24.9%)	0.17 ± 0.09	PDC (AG045D, 200 a BP)

Table 1 Radiocarbon dates of palaeosols between (scoria) fall deposits and charcoal entrained in PDC deposits. Samples are grouped by section, separated by grey horizontal bars. Analysis was performed at Beta Analytic Inc. (Florida, USA), either by conventional radiometric or AMS (Accelerator Mass Spectrometry) methods. Dates were calibrated using the IntCal13 calibration curve (Reimer et al. 2013) in OxCal 4.2 (Bronk Ramsey 2009). Calibrated ages reported at the 95.4% probability range. Samples are listed in stratigraphic order for each (composite) section, with the stratigraphically youngest sample on top. "Stratigraphic Unit" column indicates relation to immediately

underlying, immediately overlying or enclosing deposits which were analysed for bulk geochemical composition (Supplementary Table 1, Fig 3).